HHS Public Access

Author manuscript

Mol Cell. Author manuscript; available in PMC 2017 November 29.

Published in final edited form as:

Mol Cell. 2015 January 22; 57(2): 273–289. doi:10.1016/j.molcel.2014.11.016.

Yeast PP4 Interacts with ATR Homolog Ddc2-Mec1 and Regulates Checkpoint Signaling

Nicole Hustedt[1,2], **Andrew Seeber**[1,2], **Ragna Sack**[1], **Monika Tsai-Pflugfelder**[1], **Bhupinder Bhullar**[3], **Hanneke Vlaming**[4], **Fred van Leeuwen**[4], **Aude Guénolé**[5], **Haico van Attikum**[5], **Rohith Srivas**[6], **Trey Ideker**[6], **Kenji Shimada**[1,7], and **Susan M. Gasser**[1,2,7,*]

[1]Friedrich Miescher Institute for Biomedical Research, Maulbeerstrasse 66, 4058 Basel, Switzerland [2]Faculty of Sciences, University of Basel, 4056 Basel, Switzerland [3]Novartis Institutes for Biomedical Research, Novartis Pharma AG, Fabrikstrasse 22, 4056 Basel, Switzerland [4]Division of Gene Regulation, The Netherlands Cancer Institute, Plesmanlaan 121, 1066 CX Amsterdam, the Netherlands [5]Department of Toxicogenetics, Leiden University Medical Center, Einthovenweg 20, 2333 ZC Leiden, the Netherlands [6]Departments of Bioengineering and Medicine, University of California, San Diego, La Jolla, CA 92093, USA

SUMMARY

Mec1-Ddc2 (ATR-ATRIP) controls the DNA damage checkpoint and shows differential cell-cycle regulation in yeast. To find regulators of Mec1-Ddc2, we exploited a *mec1* mutant that retains catalytic activity in G2 and recruitment to stalled replication forks, but which is compromised for the intra-S phase checkpoint. Two screens, one for spontaneous survivors and an E-MAP screen for synthetic growth effects, identified loss of PP4 phosphatase, *pph3*Δ and *psy2*Δ, as the strongest suppressors of *mec1-100* lethality on HU. Restored Rad53 phosphorylation accounts for part, but not all, of the *pph3*Δ-mediated survival. Phosphoproteomic analysis confirmed that 94% of the *mec1-100*-compromised targets on HU are PP4 regulated, including a phosphoacceptor site within Mec1 itself, mutation of which confers damage sensitivity. Physical interaction between Pph3 and Mec1, mediated by cofactors Psy2 and Ddc2, is shown biochemically and through FRET in subnuclear repair foci. This establishes a physical and functional Mec1-PP4 unit for regulating the checkpoint response.

Graphical Abstract

*Correspondence: susan.gasser@fmi.ch.
[7]Co-senior author

SUPPLEMENTAL INFORMATION

Supplemental Information includes Supplemental Experimental Procedures, seven figures, and seven tables and can be found with this article online at http://dx.doi.org/10.1016/j.molcel.2014.11.016.

AUTHOR CONTRIBUTIONS

N.H. planned, performed, and evaluated most experiments; made all figures; and wrote the paper. A.S. performed FRET studies; R. Sack performed mass spectroscopy; M.T.-P. performed β-galactosidase assays; B.B. sequenced yeast mutants; H.V., F.v.L., A.G., H.v.A., T.I., and R. Srivas helped with E-MAP studies; K.S. and S.M.G. supervised and helped write the paper.

ACCESSION NUMBERS

The mass spectrometry proteomics data have been deposited to the ProteomeXchange Consortium (http://www.proteomexchange.org) (Vizcaino et al., 2014) via the PRIDE partner repository (http://www.ebi.ac.uk/pride) with the data set identifier PXD001492.

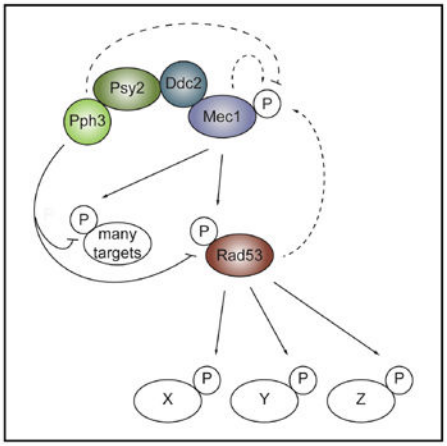

INTRODUCTION

Cells are constantly exposed to DNA damage. Lesions can arise either from exogenous agents (e.g., DNA damaging drugs) or endogenous events (e.g., replication forks encountering barriers) (Aguilera and García-Muse, 2013). DNA damage checkpoints sense damage, stop the cell cycle, and induce DNA repair events in order to preserve genome integrity (Friedel et al., 2009). Key to these signaling cascades are the PI3K-like kinases (PI3KK) ATM and ATR, or Tel1 and Mec1 in budding yeast (Cimprich and Cortez, 2008).

Whereas ATM is primarily activated in response to DNA double strand breaks (DSBs), ATR can sense a variety of lesions (Cimprich and Cortez, 2008). Most ATR activation appears to involve single-stranded (ss)DNA coated by the ssDNA binding protein replication protein A (RPA). The ATR interacting protein, ATRIP (Ddc2 in yeast), is needed to bind ssDNA (Zou and Elledge, 2003), whereas the Rad17-RFC2-5 clamp loading complex (Rad24-Rfc2-5 in *S. cerevisiae*) recognizes a double-stranded (ds)DNA adjacent to ssDNA structure and indirectly recruits TopBP1 (*S.c.* Dpb11) to further activate ATR/Mec1 (Mordes et al., 2008).

Once activated, the yeast Mec1 kinase phosphorylates the downstream kinases Rad53 and Chk1 in a manner dependent on mediator proteins. In the case of Mec1 activation in response to DSB or DNA adducts (methyl methanesulfonate [MMS] treatment), the checkpoint protein Rad9 (53BP1 in mammals) recruits Rad53 and facilitates its phosphorylation, while in response to hydroxyurea (HU)-induced replication stress, the fork components Mrc1 and Sgs1 promote Rad53 activation by Mec1 (Hustedt et al., 2013). In S phase cells, higher levels of damage are required to activate the Mec1-dependent checkpoint, suggesting an activation threshold for the intra-S checkpoint (Shimada et al., 2002; Tercero et al., 2003). This threshold may ensure that the ssDNA found at normal replication forks does not trigger the checkpoint response.

Whereas Mec1 activation has been studied extensively, how the replication checkpoint is downregulated and/or modulated to prevent unwarranted checkpoint induction is not well understood. A number of phosphatases have been shown to dephosphorylate Rad53, and it is proposed that the phosphatase used depends on the type of lesion that provokes Rad53

activation (Heideker et al., 2007). For instance, the PP1 phosphatase Glc7 was reported to promote Rad53 dephosphorylation after exposure to HU (Bazzi et al., 2010), while the PP2C phosphatases Ptc2 and Ptc3 appear to dephosphorylate Rad53 after a DSB response (Leroy et al., 2003). The PP4 phosphatase Pph3-Psy2 was implicated instead in checkpoint recovery after MMS treatment (O'Neill et al., 2007; Szyjka et al., 2008), although Ptc2/3 may compensate for loss Pph3 and vice versa during recovery fromMMS treatment or DSBs (Kim et al., 2011; Travesa et al., 2008). Finally, PP4 was also implicated in the dephosphorylation of Mec1 substrates Zip1 (Falk et al., 2010), Cdc13 (Zhang and Durocher, 2010), Cbf1 (Bandyopadhyay et al., 2010), and histone H2A (Keogh et al., 2006).

In human cells, the data on phosphatases and checkpoints are no less complicated: both downstream kinases CHK1 and CHK2 are counteracted by both the PP2C (Wip1) and PP2A phosphatases, while PP4 was shown to dephosphorylate γH2AX (phosphorylated H2AX) (Chowdhury et al., 2008; Freeman and Monteiro, 2010; Nakada et al., 2008). PP4 was also implicated in dephosphorylation of RPA2 in *C. albicans* and mammals (Lee et al., 2010; Wang et al., 2013), as well as mammalian 53BP1, KAP1, and CHD4 (Lee et al., 2012, 2014). Other mechanisms that downregulate the checkpoint act by degrading Mrc1 or human CLASPIN (Fong et al., 2013; Mailand et al., 2006; Peschiaroli et al., 2006), or by sequestering Rad9 by Rtt107-Slx4 in yeast (Ohouo et al., 2013). To date, however, no study has examined whether Mec1-Ddc2 activity itself is under negative control.

Here, we describe an interaction between the Mec1-Ddc2 checkpoint kinase and the yeast PP4 phosphatase Pph3-Psy2. A strong genetic relationship between mutants in the two complexes was identified in forward and reverse genome-wide genetic screens. We find that Mec1-Ddc2 and PP4 coregulate many Mec1-dependent phosphorylation targets in response to HU stress, including Rad53 and H2A, suggesting that this interaction maintains a balance of phosphorylation that is important for surviving fork-associated stress. We also identify a phosphoacceptor site within Mec1 that is regulated in a Pph3-dependent manner, mutation of which compromises survival of Zeocin-induced damage.

RESULTS

Spontaneous *mec1-100* Suppressor Mutations Map to *PSY2* and *PPH3* Genes

To study how the replication checkpoint is controlled, we used a mutant allele of the checkpoint kinase Mec1, *mec1-100*, which shows a delayed activation of Rad53 in S phase cells, but robust Rad53 phosphorylation in G2 (Paciotti et al., 2001). This allele carries two mutations outside of the catalytic domain, N1700S is within and F1179S is flanking the FAT domain (Paciotti et al., 2001). The kinase activity of the mec1-100 kinase is intact: the mutant kinase recovered from cell lysates by coprecipitation with Ddc2-GFP, phosphorylates a target peptide (Sgs1 amino acids [aa] 404–604) (Hegnauer et al., 2012) as efficiently as wild-type Mec1 (Figure S1A available online). Mec1-100-Ddc2 recruitment to stalled forks is equivalent to that of wild-type Mec1-Ddc2, yet the mutation compromises the recovery of engaged polymerases near stalled forks and fails to prevent late origin firing on HU (Cobb et al., 2005). Its synthetic defects in combination with *sgs1*Δ are not mimicked by *rad53*Δ, which argues that the Mec1-100 kinase fails to phosphorylate a select set of S phase specific targets that ensure survival of replicative stress.

When plated on HU, spontaneous suppressor mutations arise quite frequently in *mec1-100* cells, but not in *mec1*Δ strains (Figure 1A, full list of yeast strains in Tables S1 and S2). Since suppression could stem from either loss of negative regulators or upregulation of downstream Mec1 targets, we analyzed 31 suppressor colonies by sequencing, after backcrossing 2–3 times with the parental wild-type strain. The suppressors fell into two classes: those that cosegregated with the *MEC1* locus ("intragenic"), and those that segregated independently ("extragenic"). All intragenic suppressors had acquired one additional mutation in *mec1-100*, rendering the cells HU-resistant (Figures 1B and S1B). Remarkably, genome-wide sequencing showed that all 12 extragenic suppressor mutations were in one of two genes, *PSY2* or *PPH3*, which encode subunits of the PP4 phosphatase (Figures 1B and S1C). In the catalytic subunit, *PPH3*, mutations occurred throughout the coding region; while in *PSY2* we detected premature STOP codons at aa 40 or aa 183 (Figure 1B). All alleles were recessive, as HU sensitivity was restored to *psy2* or *pph3* double mutants with *mec1-100*, after transformation with wild-type *PSY2* or *PPH3* genes (data not shown).

Epistatic Miniarray Profiling Groups *mec1-100* with Replication Checkpoint Deficient Mutations

To better characterize *mec1-100* effects, we performed a high-throughput genetic interaction screen based on the previously described Epistatic Miniarray profiling (E-MAP) method (Collins et al., 2006, 2007). We combined 35 query strains bearing mutations in 35 genes implicated in DNA replication fork or checkpoint function, with an array of 1,525 deletions and a few decreased abundance by mRNA perturbation (DAmP) mutants, all representing functions that are required for chromatin-based processes (Guénolé et al., 2013) (Table S3). The resulting double mutants were scored for their growth in the presence of 0, 20, and 100 mM HU, and quantitative genetic interaction scores were calculated (Collins et al., 2006) (Figure 1C). A positive score indicates suppression (or potentially, epistasis), while a negative score shows synthetic sickness or synthetic lethality. Quality control of the data led to the exclusion of 214 mutants (see Supplemental Experimental Procedures), yielding a network of 45,885 (35 × 1,311) genetic interactions (Table S4).

We first compared the overall genetic interaction profile of *mec1-100* with the profiles of the other query mutants. Mutants with similar genetic interaction profiles often indicate shared function (Collins et al., 2007). As expected, the *mec1-100* profile was highly correlated with mutants that compromise the S phase checkpoint (i.e., *sgs1*Δ, *rad24*Δ, *rad17*Δ, *ddc1*Δ, *mrc1*Δ, and *dcc1*Δ ; Figure 1D). The replication checkpoint mediator, *mrc1*Δ, showed the strongest correlation with *mec1-100* in the presence of HU, yet did not correlate in its absence, arguing that the proteins cooperate on HU, but function distinctly in an unperturbed S phase (Figure 1D). These S phase checkpoint mutants also show negative genetic interactions with *mec1-100* (Figures 1C, S1D, and S1E). Thus, they most likely act on parallel pathways that achieve the same function as *mec1-100*, or else on the same pathway in a redundant fashion (Figure 1C).

Interestingly, there are two groups of mutants whose genetic correlation patterns change dramatically upon HU treatment. Profiles of mutants that compromise break-induced

replication or translesion synthesis (i.e., *rad18*Δ, *slx5*Δ, *slx8*Δ, *mre11*Δ, *rad52*Δ, and *bre1*Δ) correlate with *mec1-100* only in the presence of HU, while the opposite was observed for *rad9*Δ, *dot1*Δ, *sae2*Δ, *yku70*Δ, and *sgs1-r1*Δ (Hegnauer et al., 2012), which confer selective sensitivity to Zeocin. These genetic interaction profiles suggest that in the absence of HU, *mec1-100* cells are somewhat compromised for DSB repair, while on HU, replication fork stabilization and recovery are lost. Indeed, even on HU, the specific mutants that interact with *mec1-100* (based on threshold scores ≥2 for suppressive and ≤−2 for negative interactions) fall into distinct functional groups (Figures 1C and S1D, discussed in legend). However, of the 1,311 mutants scored, *psy2*Δ and *pph3*Δ showed the highest suppressive genetic interaction with *mec1-100*, and clearly promoted survival on HU (Figures 1C and S1D; Table S4).

PP4 Subunits Psy2 and Pph3 Counteract *mec1-100* Sensitivities

Given that two independent screens show that loss of Psy2 or Pph3 robustly suppresses *mec1-100* lethality on HU, we studied these factors in depth. Psy2 and Pph3 form the PP4 phosphatase, with Pph3 as the catalytic subunit (Gingras et al., 2005). We first showed that the suppression of *mec1-100* by *pph3*Δ indeed reflects loss of phosphatase activity, since the catalytically inactive mutant, *pph3-H112N* (O'Neill et al., 2007), supports *mec1-100* growth on HU to the same extent as *pph3*Δ (Figure 2B).

Because both the E-MAP and past experiments had implicated multiple phosphatases in yeast checkpoint control (Figure 2A), we created double mutants in a second yeast background (W303) of *mec1-100* with other phosphatase genes and scored for survival of HU stress (Figure 2C). The E-MAP suggested that the loss of PP5 phosphatase (*ppt1*Δ), like those of the PP2A phosphatase (*pph21*Δ, *pph22*Δ, *sap155*Δ, *sap185*Δ, *sap190*Δ, and *sap33*Δ), had no genetic interaction with *mec1- 100* (Figure 1C). On the other hand, loss of Rrd2, which interacts with and regulates PP2A, or Rrd1, a binding partner of Pph3 (PP4), like Ppg1 (related to PP4 and PP6) and Sit4 (PP6) (Van Hoof et al., 2005), did show low level suppression by E-MAP (Figure 1C). These latter effects, however, were extremely weak when deletions were recreated in W303 (Figure 2C), as was loss of Ptc2 (one of seven PP2C proteins; Figure 2C). We also could rule out robust effects of other PP2C mutants (*ptc1*Δ and *ptc4*Δ) and of a phosphotyrosyl phosphatase mutant *oca1*Δ, which showed little or no suppression of *mec1-100* in W303 on HU (Figure 2C).

Deletions of *PPH3* or *PSY2* Counteract Failed Replication Fork Recovery in *mec1-100* Cells

Previous work suggested that PP4 dephosphorylates the checkpoint effector kinase Rad53 in a manner that is redundant with Ptc2 and Ptc3 (PP2C-type phosphatases) and the PP1-type phosphatase, Glc7, depending on the type of damage that activated the checkpoint (Bazzi et al., 2010; Heideker et al., 2007; Leroy et al., 2003; O'Neill et al., 2007; Travesa et al., 2008) (Figure 2A). Indeed, it was reported that Pph3 was dispensable for Rad53 dephosphorylation after HU arrest, while Glc7 was not. However, in the context of the HU-induced checkpoint in *mec1-100*, neither the partial loss of function allele *glc7-132* (Bazzi et al., 2010), nor *ptc2* or *ptc3* deletions, showed significant suppression of HU-induced lethality (Figure 2C). Thus, Glc7 and Ptc2/Ptc3 probably counteract responses stimulated by conditions other than HU.

Previous work suggested that Rrd1 and Pph3 act on the same pathway at DSBs to dephosphorylate the Mec1 target Cdc13 (Zhang and Durocher, 2010). Therefore, we tested *rrd1*Δ epistasis with *pph3*Δ in triple mutants. Surprisingly, the coupling of *rrd1*Δ with *psy2*Δ or *pph3*Δ reduced the suppression of *mec1- 100* sensitivity to HU (Figure 2D), arguing that *rrd1*Δ interferes with suppression by *psy2*Δ or *pph3*Δ, while both the *pph3*Δ *ptc2*Δ and *pph3*Δ *psy2*Δ double mutants suppressed in an additive fashion. We conclude that Rrd1 counteracts *mec1-100* lethality on HU in a manner distinct from PP4 (Figure 2D).

To shed more light on how PP4 suppresses *mec1-100* lethality on HU, we checked whether stalled replication forks remain engaged in the phosphatase mutants, allowing fork restart upon HU removal. When pheromone synchronized cultures are released into S phase on HU, *mec1-100* cells suffer a partial loss of replicative polymerase engagement at sites of early replication and show reduced recovery upon removal of HU (Cobb et al., 2005). We tested single and double mutants of PP4 and PP2C with *mec1-100*, and scored for recovery after release from a synchronous arrest in S phase, both in the presence and absence of Tel1 (Figures 2E and 2F). The combination of *pph3*Δ with *mec1-100* robustly rescued the defect, particularly at early time points (1–2 hr, Figure 2E), while *ptc2*Δ had a weaker effect, particularly in the absence of Tel1 (Figure 2F). We conclude that loss of Pph3 efficiently suppresses both the HU sensitivity and fork recovery defects of *mec1-100*, without recourse to the Tel1/DSB checkpoint response.

Rad53 Activation Correlates with High Levels of Suppression

In the checkpoint cascade, Rad53 is activated by Mec1-mediated phosphorylation, which is compromised in *mec1-100* strains (Paciotti et al., 2001). Given that Ptc2 and Pph3 were both implicated in Rad53 dephosphorylation under other conditions (Travesa et al., 2008), we tested whether the reduced S phase level of Rad53 phosphorylation found in *mec1-100* cells is counteracted by loss of Pph3 or Ptc2. Cells bearing *mec1- 100* in combination with *pph3*Δ or *ptc2*Δ were pheromone synchronized in G1 and released into S phase in the presence of HU. Western blots showed the characteristic delay in Rad53 activation in the *mec1-100* background; this was compensated by *pph3*Δ or more weakly, by *ptc2*Δ (Figure 3A). By performing all assays in a *tel1*Δ background, we could exclude that the observed suppression stems from compensation by Tel1 (Figures 3B and S2A). Neither *ptc2*Δ nor *pph3*Δ influenced Rad53 activation kinetics in $MEC1^+$ cells (Figure 3A), although in both $MEC1^+$ and *mec1-100* backgrounds, Rad53 remained more robustly phosphorylated at 90 min when Pph3 was ablated, than with loss of Ptc2, with very pronounced differences by 120 min after HU removal (Figures 3A, 3B, S2A, and S2B). Nonetheless, this delay in Rad53 dephosphorylation does not compromise survival in the recovery assay, while the efficiency of activation does (Figure 2E).

In these assays, *ptc2*Δ had effects similar to *pph3*Δ, although generally less pronounced (Figures 2 and 3). Consistent with the notion that PP4 acts by dephosphorylating targets of checkpoint kinases, we found that Tel1 was necessary in a *mec1* null for *pph3*Δ to exert its suppressor effect, although it was not necessary in *mec1-100*, which retains residual Mec1 kinase activity (Figures 3C, 3D, and S1A). In conclusion, the correlation between Rad53

activation kinetics and the suppression of HU sensitivity argues that *pph3*Δ suppresses *mec1-100*, at least partly by regulating the efficiency of Rad53 activation.

PP4 Targets Rad53 and Other Factors to Mediate *mec1-100* Suppression

Rad53 initiates many of the downstream checkpoint responses on HU (e.g., cell cycle arrest and late origin firing), yet there is extensive evidence that Mec1 has unique roles in the replication checkpoint that are independent of Rad53 (Hustedt et al., 2013). To see if the suppression of *mec1-100* by *pph3*Δ involves targets beyond Rad53, we asked whether *pph3*Δ can suppress *mec1- 100* in the absence of Rad53. To avoid *rad53*Δ lethality, we coupled it with a bypass mutation, *sml1*Δ (Zhao et al., 1998), generating a strain that is extremely sensitive to HU. Nonetheless, serial dilution of the *mec1-100 rad53*Δ *sml1*Δ mutant on plates with low HU concentrations revealed a mild, but reproducible increase in survival upon deletion of *PPH3* (Figure 3E). This was also true in the absence of Chk1 (Figure 3F). Thus, while Rad53 plays an important role, the phosphorylation status of proteins other than Rad53 and Chk1 also help rescue the *mec1-100* lethality on HU. This residual suppression was not observed in *rad53*Δ *mec1*Δ *sml1*Δ cells, indicating again that the remaining kinase activity of *mec1-100* is required for *pph3*Δ suppression. This underscores the crucial role of Mec1, and not Tel1, in HU survival. In conclusion, activation of the downstream kinase Rad53 is important, but is not the only Mec1-mediated phosphorylation event enhanced by loss of PP4, ensuring *mec1-100* growth on HU.

Restoration of H2A Phosphorylation Does Not Correlate with Suppression

A known target of Pph3 (PP4) during the DNA damage response in both yeast and mammals is histone H2A/H2AX (Chowdhury et al., 2008; Keogh et al., 2006; Nakada et al., 2008). Yeast H2A is phosphorylated on Serine 129 by Mec1 and/or Tel1 at DSBs and stalled replication forks (Cobb et al., 2005; Downs et al., 2000; van Attikum et al., 2004). We confirmed that H2A phosphorylation levels were increased by *PPH3* or *PSY2* deletion in both wild-type (WT) and *mec1-100* backgrounds after treating S phase cells with HU (Figure S2D). However, unlike Rad53, phospho-H2A regulation is not only dependent on Pph3 and Psy2, but also on Psy4, a variable third subunit of the complex (Keogh et al., 2006; O'Neill et al., 2007). Given that loss of Psy4 did not rescue *mec1-100* HU sensitivity in WT or *rad53*Δ *sml1*Δ backgrounds (Figures 1C, 2C, and S2C), we conclude that enhanced H2A phosphorylation cannot be responsible for the rescue of *mec1-100* cells on HU.

Phosphopeptides Downregulated in *mec1-100* Cells Are Upregulated by *pph3* Deletion

To find the Mec1 targets that are responsible for *mec1-100* suppression on HU, we performed a quantitative phosphoproteomic study. Specifically, we screened for modifications that are downregulated in *mec1-100*, compensated by *pph3*Δ, and left unaffected by *rad53*Δ (Figure 4A). To eliminate contributions from Tel1 (Figures 2E, 2F, 3A, and 3B), we used a *tel1*Δ *mec1-100* double mutant in the screen. Prior to extraction of proteins, the cultures were arrested in G1 by α factor and released into S phase in the presence of HU (Figure 4B).

There were 2,368 phosphopeptides that could be quantified (Table S5), of which 47 were specifically reduced in *mec1-100 tel1*Δ, but not in *rad53*Δ *sml1*Δ, cells (Figure 4C; Table

S6). Among them were the repair factor Rdh54, chromatin remodeler INO80 subunit Ies4, the mismatch repair protein Msh6, and transcription regulators like Swi3 and Leo1, the latter being a component of the PAF1 complex (Figure 4C). We did not find any proteins known to control DNA replication. Remarkably, however, when the abundance of these phosphopeptides was scored after deletion of *PPH3*, almost the entire set was upregulated (i.e., 94% showed restored phophosphorylation in *mec1- 100 tel1*Δ *pph3*Δ versus *mec1-100 tel1*Δ ; Figure 4D). This effect, averaged over all mec1-100-dependent targets, is both highly significant (Figure 4D, inlay) and specific, because it was not observed when the entire population of quantified phosphopeptides was compared ±Pph3 (Figure S3A). Remarkably, the loss of Pph3 balances out almost all of the phosphorylation defects that we detect in *mec1-100* cells on HU. This supports our genetic results, which showed opposing functions for these two mutations (Figure 1).

Serine/Threonine followed by Glutamine (Q) Phosphopeptides Are Upregulated in *rad53*Δ, but Are Unaffected by *mec1-100*

Among the 47 phosphopeptides that were specifically downregulated in the *mec1-100 tel1*Δ mutant, only a few (ten phosphopeptides) fit the generally assumed ATR/ATM consensus p[S/T]Q (Kim et al., 1999). This could reflect technical problems in our detection of serine/threonine followed by glutamine (Q) (S/TQ) sites, or simply arise because S/TQ-containing peptides did not match the stringent criteria we applied to identify *mec1-100 tel1*Δ -dependent phosphopeptides. We therefore triaged for phosphopeptides that were less abundant in *mec1-100 tel1*Δ versus *rad53*Δ *sml1*Δ cells ($\log_2$ ratio ≤−1, p value ≤ 0.05), regardless of their abundance in WT cells, and screened independently for known Mec1/Tel1 targets (Chen et al., 2010). Using this approach, we identified many p[S/T]Q phosphopeptides in our phosphoproteomic data set, including known fork-associated Mec1/Tel1 targets such as Rfa2 (Brush et al., 1996) and H2A (Downs et al., 2000) (Figures S3B and S3C; Table S7). These hits were eliminated in our earlier analysis because they were not downregulated in *mec1-100 tel1*Δ cells versus WT. Thus, mec1-100 kinase is actually proficient for phosphorylating many S/TQ Mec1 targets on HU, consistent with the robust kinase activity we detect in the pull-downassay (Figure S1A). These S/TQ acceptor sites are, therefore, unlikely to be responsible for the *mec1-100* lethality on HU.

Intriguingly, the majority of p[S/T]Q phosphopeptides that we recovered in the second analysis were more abundant in the *rad53*Δ *sml1*Δ mutant than in WT cells, and they were not further affected by loss of Pph3 (Figures S3C–S3E). This suggests that in *rad53*Δ *sml1*Δ cells, Mec1 and/or Tel1 may be hyperactivated on HU, either because the cells accumulate additional DNA damage at the fork, or because they lose a negative feedback loop through which Rad53 normally downregulates Mec1 activity.

Mec1-Ddc2 and Pph3-Psy2 Physically Interact in a DNA Damage-Independent Manner

From our phosphoproteome analysis, we conclude that almost every phosphopeptide (94%) that was reduced due to the *mec1-100* mutation was restored by further elimination of Pph3, in the absence of Tel1. How could this robust coordination be guaranteed? We speculated that the Mec1 kinase and PP4 phosphatase might bind each other to ensure coordinated action. To test this, we created yeast strains that expressed epitope-tagged versions of the

kinase or phosphatase subunits from their native genomic loci. Whereas the tagged Psy2 and Ddc2 forms were fully functional, tags on Mec1 or Pph3 rendered cells slightly sensitive to MMS or HU (Figures S4A–S4D). Since Ddc2-Mec1 and Psy2-Pph3 are both stable complexes (Gingras et al., 2005; Paciotti et al., 2000), we used the functional tagged versions of Psy2 or Ddc2 in subsequent assays. As positive and negative controls, we tested for interaction with Rfa1 and Ptc2.

Consistent with our hypothesis, immunoprecipitation (IP) of Ddc2-GFP efficiently recovered Psy2-MYC, but not Ptc2 (Ptc2-PK; Figures 5A and S4E). The Psy2-Ddc2 interaction is not compromised by removal of nucleic acids with benzonase and RNaseA (Figure 5A), whereas Ddc2-GFP-Rfa1 signals were sensitive to this treatment (Figure 5A). The Ddc2-GFP/Psy2-MYC interaction was also independent of HU, being scored both in untreated G1- and in treated S phase cells, and the IP worked reciprocally (Figures 5B and S5B). Finally, the robust Ddc2-Psy2 interaction did not require Pph3 or Mec1 and was not affected by the *mec1-100* mutant (Figures 5B and S5A).

The interaction was further mapped by yeast-two hybrid, through which we could define the minimal Psy2 domain (aa 130–350) that robustly binds Ddc2 (Figures 5C and S5C). Although a smaller Psy2 fragment (aa 130–350) only weakly binds Ddc2, its deletion fully abolished the interaction. Another robustly expressed Psy2 fragment (aa 25–129; Figure S5D) failed to interact significantly, although its deletion reduced the interaction by about 50%.

Ddc2-Psy2 Homologs Interact in Mammalian Cell Extracts

Psy2 has two human homologs, PP4R3A and PP4R3B, which share an overall sequence similarity with Psy2 of 37% and 44% and an identity of 24% and 22%, respectively. Intriguingly, the Ddc2 binding domain within Psy2 (aa 130–350) is highly conserved in PP4R3A (50% identity) and PP4R3B (51% identity) (Figure 5D). We therefore tested whether these regulatory phosphatase subunits bind ATRIP in human cells, following transient transfection of human embryonic kidney cells (HEK)293T cells with plasmids encoding for MYC-tagged ATRIP and either PP4R3A-GFP, PP4R3B-GFP, or GFP alone. MYC-ATRIP bound efficiently to PP4R3B-GFP, but not to GFP alone and only weakly to PP4R3A-GFP (Figure 5E), even though PP4R3A expression levels were much higher. Thus, the PP4R3B-ATRIP interaction is strongly preferred. We conclude that in budding yeast and human cells Ddc2/ATRIP binds the phosphatase subunit Psy2/PP4R3B, and thus kinase and phosphatase appear capable of forming a complex. In yeast, the interaction involves a conserved N-terminal region of Psy2, and is HU-, Mec1-, and Pph3-independent.

Ddc2 and Psy2 Interact and Colocalize in Nuclear Foci In Vivo

Although the genetic and biochemical evidence for interaction was strong, it was unclear whether the Mec1/Ddc2-PP4 interaction occurs at the right place and the right time, i.e., at stalled replication forks or sites of damage. To localize the putative complex in living cells, we fused Psy2, Ddc2, and Rfa1with distinct fluorescent proteins (RFP, GFP, and CFP, respectively). All fusions were expressed under their endogenous promoters from their genomic loci and were fully functional (Figures S4A, S4D, and S4F). As expected, Rfa1-

CFP has a punctate nuclear signal in S phase cells, consistent with the existence of replication foci (Pasero et al., 1997) (Figures 6A and 6B). Whereas the abundance of Rfa1 renders Rfa1-CFP replication foci difficult to resolve in yeast, both Ddc2-GFP and Psy2-RFP formed foci that were larger and less numerous, even in untreated S phase cells (Figures 6A and S6A), most likely indicating repair foci. Indeed, consistent with previous reports, Rfa1/Ddc2 foci were also detected in G1-phase cells, albeit rarely (Figure S6A) (Lisby et al., 2004).

Following incubation with HU, Rfa1, Ddc2, and Psy2 concentrated in intense nuclear foci (Figure 6B), allowing us to score both their number and colocalization (Figures 6C, 6D, and S6C– S6F). Approximately 15% of untreated S phase cells contained a single bright focus of Rfa1 and/or Ddc2, likely indicative of spontaneous damage, while Psy2-RFP occasionally formed two (Figure 6C). On HU, on the other hand, we frequently scored >2 Ddc2 or Psy2 foci per cell (Figure 6C). We quantified the degree of colocalization of the tagged proteins on HU and found that 70% of the Rfa1 foci coincided with both Ddc2 and Psy2, while an additional 20% contained only Rfa1 and Ddc2 (Figure 6D). There were about 70% of the Ddc2 foci that also contained Psy2 (Figure 6D). In cells treated with 400 μg/ml Zeocin, a radiomimetic drug that induces both ssDNA lesions and DSBs, extensive foci containing both Rfa1 and Ddc2 foci were scored (Figures S6B–S6E); strikingly, Psy2 colocalized with Rfa1 primarily when Ddc2 was present (~60% of the brightest foci, Figure S6F).

To go beyond the limited resolution of confocal microscopy, we used the tagged constructs to score Förster resonance energy transfer (FRET), which monitors the energy transfer between donor (GFP) and acceptor (RFP) fluorescent proteins, if they are ≤10 nm apart (Figure 6E) (Piston and Kremers, 2007). We used four FRET pairs (Ddc2-GFP/Psy2-RFP; Ddc2-GFP/Rfa1-RFP; Psy2-GFP/Rfa1-RFP; and Rfa2-GFP/Psy2-RFP). This revealed highly significant FRET signals between Ddc2- GFP and Psy2-RFP at the bright foci in S phase cells on HU, suggesting that Mec1-Ddc2 and PP4 are indeed in very close proximity in vivo, at the time and place necessary for *mec1-100* suppression. The interaction between Ddc2 and Rfa1 is also substantial, while Psy2-Rfa1 FRET signals were less strong (Figure 6F). This argues that Ddc2-Psy2 interact at stalled or collapsed fork foci. We scored similar FRET results after treatment with Zeocin or at spontaneous bright foci in untreated cells (Figure 6F, Psy2-Rfa2 data not shown), whereas there is no observable FRET between nonfocal nuclear fractions of any of these reporter pairs. This does not exclude interactions outside of damage foci, but rather suggests that any interaction in undamaged nucleoplasm is below our detection level (Piston and Kremers, 2007). We conclude that the detected interactions between the Mec1 kinase cofactor, Ddc2, and the PP4 subunit, Psy2 occur in living cells.

Mec1 Phosphorylation on Serine 1991 Is Regulated in a Pph3-Dependent Manner

Several PP4 targets interact stably with the phosphatase (Keogh et al., 2006; Lee et al., 2010; Ma et al., 2014; O'Neill et al., 2007). Thus, we hypothesized that Pph3 might regulate Mec1, and not only counteract the enzyme by dephosphorylating its targets. To test this, we looked for phosphorylation sites in Ddc2 and Mec1 that are substrates for Pph3-Psy2. After 1 hr on HU, Mec1-Ddc2-GFP complexes were IP'd from *mec1-100* or *MEC1*$^{+}$ cells, and

phosphopeptides were analyzed by mass spectrometry. There were two residues (Ser38 and Ser1991) in Mec1 that were robustly phosphorylated in WT, but not in *mec1-100* strains (Figure 7A). While Ser38 has been described previously as a potential autophosphorylation site (Chen et al., 2010; Smolka et al., 2007), phosphorylation at Ser1991, which sits between Mec1's conserved FAT and kinase domains, has not been reported to date. A number of intragenic suppressor mutations in *mec1-100* map to this region (Figures 1B and 7A), and the mammalian ATR kinase has a nearby autophosphorylation site at Thr1989 (Liu et al., 2011; Nam et al., 2011).

Using a phospho-specific Ser1991 antibody on extracts from HU-treated cells, we detected Mec1, but not mec1-S1991A, on a blot after precipitation with Ddc2-GFP (Figure 7B). Ser1991 phosphorylation is elevated on HU, is not detected in an unperturbed S phase, shows a slight enhancement on Zeocin, and was virtually absent in the *mec1-100* strain (Figures 7B and 7C). Importantly, Ser1991 phosphorylation could be restored in *mec1-100* cells by deleting *PPH3*, indicating that PP4 indeed regulates Mec1 phosphorylation, compensating for the *mec1-100*-associated loss of S1991 modification (Figure 7D).

Mec1 Ser1991-phosphorylation was absent in a catalyticdead Mec1 protein, yet also in a strain lacking Rad53 (Figure 7D). This suggests that Ser1991 requires both Mec1 and Rad53 for its phosphorylation, although it remains unclear whether either acts directly. We attempted to demonstrate direct dephosphorylation of Ser1991 in vitro using Pph3-Psy2 isolated from cells expressing Psy2-Halo (Figure S7A), but the precipitated Pph3-Psy2 could not dephosphorylate the appropriate Mec1 peptide, even though a nonspecific enzyme, calf intestinal alkaline phosphatase, could dephosphorylate both Cdc13 and Mec1 peptides in vitro and Pph3-Psy2 was able to dephosphorylate Cdc13 (Zhang and Durocher, 2010) (Figure S7B). We cannot exclude that our conditions were inappropriate to monitor dephosphorylation of Ser1991, yet it appears that it is not a preferred substrate of Pph3-Psy2 in vitro.

Surprisingly, the *mec1-S1991A* mutant showed impaired growth in the presence of Zeocin, but not on HU, MMS, UV, or γ-irradiation (Figures 7E and S7C). This effect is independent of Ser38. We further confirmed the sensitivity of *mec1-S1991A* cells to induced DSBs by ectopically expressing EcoRI in all strains. Indeed, the *mec1-S1991A* mutant showed EcoRI-sensitivity (Figure 7F), while *mec1-S1991D* had a slight resistance. Consistently, the *mec1-S1991A* mutant shows a strong synergistic genetic interaction with deletion of the DNA damage checkpoint protein Rad9 and additive interactions with other checkpoint mutants *rad24*Δ, *ddc1*Δ, and *mrc1-AQ* (Osborn and Elledge, 2003), and DSB repair mutants *rad51*Δ and *dnl4*Δ (Figure S7D). If Mec1 S1991 were the only target site through which Pph3 regulated Mec1 function, the nonphosphorylatable *mec1-S1991A* mutant should suppress *pph3*Δ defects. This was not the case, indicating that there are other sites in Mec1 or Ddc2 through which Pph3 might regulate Mec1-Ddc2 activity (Figure S7E). Future studies should clarify the molecular details of this regulation pathway.

DISCUSSION

We show that the central checkpoint kinase Mec1-Ddc2 (human ATR-ATRIP) forms a stable complex with the PP4 (Pph3-Psy2) phosphatase. The two enzymes act in a coordinated, yet opposing, manner on a large number of substrates (Figure 7G). The modification of this target set is compromised in the S phase-specific Mec1 mutant, *mec1-100*, which confers hypersensitivity to replication stress. The sensitivity of *mec1-100* to HU is, however, efficiently suppressed by *pph3*Δ or *psy2*Δ. PP4 also counteracts a phosphoacceptor site on Mec1 itself, which is sensitive to the *mec1-100* mutation (Figure 7H). In vivo FRET studies then confirmed that Mec1-Ddc2 and PP4 interact at sites of replication fork-induced damage and at DSBs (Figure 6). Although the majority (70%) of the Ddc2 foci colocalize with Psy2, this does not allow us to draw conclusions about the fraction of Mec1-Ddc2 in the cell that is bound to PP4. We do not exclude that Mec1-Ddc2 is in complex with Pph3-Psy2 in undamaged conditions, whereby it might regulate noncheckpoint functions of the kinase.

The complex of phosphatase and kinase may allow the finetuning of ATR-ATRIP (Mec1-Ddc2) for different functions through the cell cycle. The fact that there seems to be a higher threshold for damage-induced checkpoint activation in S, as opposed to G2, phase, suggests that Mec1/ATR modulation is an important regulatory event in the cell cycle (Shimada et al., 2002; Tercero et al., 2003). Indeed, Mec1 not only has to react appropriately to ssDNA, but must also be switched off rapidly to allow efficient replication and cell cycle resumption. This role may be ensured by the closely associated Pph3-Psy2 complex. We show that Rad53 dephosphorylation during recovery from HU treatment is delayed in *pph3*Δ cells (Figures 3A, 3B, S2A, and S2B), although loss of PP4 did not compromise recovery from arrest, as scored by colony formation (Figures 2E and 2F). Presumably other phosphatases (Ptc2, Ptc3, or Glc7) compensate over time for the loss of PP4, as reported for recovery from MMS treatment and DSB repair (Kim et al., 2011; Szyjka et al., 2008). We and others find that *pph3*Δ is synthetic sick with *dia2*Δ, *ptc2*Δ, and *sae2*Δ on HU, which also impair recovery from checkpoint-induced arrest (Figure S1D) (Guénolé et al., 2013; Keogh et al., 2006; Kim et al., 2011; O'Neill et al., 2007; Szyjka et al., 2008). These proteins may target Rad53 (Guillemain et al., 2007; Leroy et al., 2003; O'Neill et al., 2007; Travesa et al., 2008), limit Tel1 signaling (Clerici et al., 2006), or promote Mrc1 degradation (Fong et al., 2013). In either case, loss of Ptc2 showed significantly milder effects than *pph3*Δ and does not physically interact with Mec1-Ddc2 (Figures 2, 3, and 5)

The Yin/Yang of Mec1/PP4 Complexes

The copurification of opposing enzymatic activities is not unique. We note that the human RAP80 complex contains both ubiquitin ligase and deubiquitinase enzymes (Sobhian et al., 2007), and histone acetyltransferases and deacetylases have been shown to not only create a dynamic balance of acetylation of target proteins, but also be physically associated with each other, sometimes even regulating each other's activity (Yamagoe et al., 2003). Intriguingly, Pph3-Psy2 regulates a phosphorylation site within the Mec1 kinase, Ser1991, possibly indirectly through Rad53 (Figure 7H), mutation of which compromises survival in face of DSBs, and not on HU. We have no clear explanation for this sensitivity, but note that the *mec1-100* E-MAP profile in the absence of HU shows similarity to those of genes involved

in DSB repair (Figure 1D). In fact, Ser1991 phosphorylation may alter the specificity of Mec1 and/or trigger its downregulation, rather than its induction. Intriguingly, Rad53 itself seems to be required for Mec1 Ser1991 phosphorylation, and given that we detected a large set of S/TQ phosphoacceptor peptides (Mec1 targets) that are upregulated in a *rad53* deletion strain (Figures S3C–S3E), it is possible that Rad53 controls Mec1- Ddc2 in a negative fashion. An alternative interpretation, however, is that there is more damage in *rad53*Δ cells, which indirectly triggers Mec1/Tel1 activation.

How does checkpoint activation occur if an antagonizing activity is stably associated with the activating kinase? The phosphorylation of any given protein at any given time is always the result of competing kinase and phosphatase activities. Obviously, upon checkpoint activation, the catalytic rate of phosphorylation becomes stronger, and phosphorylated proteins accumulate. It appears that once Mec1 activation is triggered, it does not matter how much stronger it is (i.e., whether Pph3 is present or not). This would explain why Pph3 does not affect phosphorylation in *MEC1*$^{+}$ cells, but does in *mec1-100*, which may have lower catalytic rates toward a subset of substrates in vivo.

The balance between the opposing activities can only be flipped by altering their specific activities. For instance, the recruitment of Rad53 by Sgs1 or Mrc1 (Alcasabas et al., 2001; Hegnauer et al., 2012) may induce a change in the specific activity of Mec1 toward Rad53, triggering checkpoint activation. Alternatively, the kinase may alter activity of the phosphatase, inhibiting it once a specific level of damage has occurred, and releasing it once damage is repaired. Finally, although we did not detect phosphopeptides from either Psy2 or Pph3, we cannot exclude that PP4 is a target of Rad53 or Mec1.

Other studies have identified DNA damage-related PP4 targets, both in yeast and in mammals, among them mammalian RPA2, KAP-1, 53BP1, CHD4, and yeast Cbf1, even though these studies were partially performed under nondamaging conditions (Bandyopadhyay et al., 2010; Lee et al., 2010, 2012). Those additional targets, and the 47 targets hit by both Mec1-Ddc2 and Pph3-Psy2 identified here, are most likely a nonexhaustive list, given that phosphopeptide coverage is rarely complete. Nonetheless, it is remarkable that 94% of the 47 phosphopeptides showing reduced phosphorylation levels in *mec1-100* responded to a deletion of *PPH3*. This corroborates our genetic data, which showed suppression of *mec1- 100* by *pph3*Δ and a strong anticorrelation of their genetic interaction profiles.

Among many other interesting genetic interactions scored for *mec1-100*, we found several subunits of the chromatin remodeling complexes INO80, SWI/SNF (Switch or Sucrose non-fermentable), ISW (Imitation SWI/SNF), and Chd1, which show HU-induced synthetic lethality with *mec1-100* (Figures 1C and S1D). Relevant to the phenotypes attributed to chromatin remodelers for stalled replication forks recovery (Papamichos-Chronakis and Peterson, 2008; Shimada et al., 2008), subunits of these chromatin remodelers were also among the *mec1-100* downregulated phosphopeptides (e.g., Ies4 and Swi3). This reflects the close relationship of remodelers such as INO80 with DNA fork associated damage, as well as their recruitment to DSBs (van Attikum et al., 2004).

A parallel study indicated two different modes of Mec1 activity, one working during unchallenged DNA replication, and one in response to damage (M. Smolka, personal communication). It is tempting to speculate that the association of Mec1-Ddc2 with Pph3-Psy2 is involved in regulating the switch between these two functions. Further work will delineate the underlying molecular mechanisms of such a switch.

EXPERIMENTAL PROCEDURES

Yeast Materials, Microscopy, Phosphoproteomics, Phosphatase Assay, and E-MAP

Yeast strains and plasmids are described in Tables S1, S2, and S3. Details of yeast two hybrid assay, growth conditions, antibodies, microscopy, phosphoproteomics, and the E-MAP assay are found in Supplemental Experimental Procedures. In general, the conditional E-MAP analysis was performed as described in Guénolé et al., 2013.

Mammalian Cell Culture

HEK293T cells were cultured in Dulbecco's modified Eagle's medium containing 10% fetal bovine serum. Transfections were carried out using jetPEI (Polyplus) transfection reagent according to manufacturer's instructions.

Spontaneous Suppressor Screening

mec1-100 (GA-4978) and *mec1-100 exo1*Δ (GA-6356) cells were plated on yeast extract, peptone, adenine, and dextrose (YPAD) + 50 mM HU and incubated for three days. Colonies were picked and backcrossed 2–3 times with WT (GA-1982) cells. Strains yielding no HU sensitive *LEU + HIS + (mec1-100*) spores were considered to have intragenic suppressors and the *MEC1* locus was sequenced. Strains yielding both HU sensitive and insensitive LEU^{+} HIS^{+} *(mec1-100*) spores were deep sequenced to find extragenic mutations. Details are in Supplemental Experimental Procedures.

Kinase and Phosphatase Assays, Recovery and Drop Assay, Rad53 and H2A Phosphorylation, Fluorescence Activated Cell Sorting, and IP

Enzymatic assays, recovery and drop assays, fluorescence activated cell sorting (FACS) analysis, and Rad53 and H2A phosphorylation analysis were done as described previously (Hustedt and Shimada, 2014) or as detailed in Supplemental Experimental Procedures. AntiGFP IP was carried out as described for kinase assays, except that the lysis buffer was supplemented with protease and phosphatase inhibitors (see Supplemental Experimental Procedures) and bead-bound protein complexes were washed three times with lysis buffer prior elution with 0.2 M glycine. IP for mammalian cells was essentially the same, except that cells were harvested 48 hr post transfection by scraping off the plate into PBS, and washed once in PBS before snap-freezing pellets in liquid nitrogen. Nuclease treatment and nucleic acid monitoring is described in online Supplemental Experimental Procedures.

Supplementary Material

Refer to Web version on PubMed Central for supplementary material.

Acknowledgments

N.H. thanks the European Union Innovative Training Networks “Image DDR” and the Swiss Cancer League for support. The Gasser laboratory is further supported by the Swiss National Science Foundation, Novartis Research Foundation, and the Human Frontier Science Program. F.v.L. and H.V. were supported by The Dutch Cancer Society and H.v.A. by the Netherlands Organization for Scientific Research (TOP-GO grant). R. Srivas is supported by the Damon Runyon Cancer Research Foundation (DRG-2187-14). We thank M.P. Longhese for strains; F.E. Romesberg for plasmids; D. Durocher for reagents; D. Hoepfner (Novartis) for E-MAP library analysis; E. Oakeley, S. Schuierer, T. Roloff, S. Dessus-Babus, and M. Stadler for deep sequencing and analysis; H. Gut and I. Deshpande for construct design; and Y. Murata, S. Nohara, M. Kawai, S. Ishikawa, and K. Doi for assistance.

References

Aguilera A, García-Muse T. Causes of genome instability. Annu Rev Genet. 2013; 47:1–32. [PubMed: 23909437]

Alcasabas AA, Osborn AJ, Bachant J, Hu F, Werler PJ, Bousset K, Furuya K, Diffley JF, Carr AM, Elledge SJ. Mrc1 transduces signals of DNA replication stress to activate Rad53. Nat Cell Biol. 2001; 3:958–965. [PubMed: 11715016]

Bandyopadhyay S, Mehta M, Kuo D, Sung MK, Chuang R, Jaehnig EJ, Bodenmiller B, Licon K, Copeland W, Shales M, et al. Rewiring of genetic networks in response to DNA damage. Science. 2010; 330:1385–1389. [PubMed: 21127252]

Bazzi M, Mantiero D, Trovesi C, Lucchini G, Longhese MP. Dephosphorylation of gamma H2A by Glc7/protein phosphatase 1 promotes recovery from inhibition of DNA replication. Mol Cell Biol. 2010; 30:131–145. [PubMed: 19884341]

Brush GS, Morrow DM, Hieter P, Kelly TJ. The ATM homologue MEC1 is required for phosphorylation of replication protein A in yeast. Proc Natl Acad Sci USA. 1996; 93:15075–15080. [PubMed: 8986766]

Chen SH, Albuquerque CP, Liang J, Suhandynata RT, Zhou H. A proteome-wide analysis of kinase-substrate network in the DNA damage response. J Biol Chem. 2010; 285:12803–12812. [PubMed: 20190278]

Chowdhury D, Xu X, Zhong X, Ahmed F, Zhong J, Liao J, Dykxhoorn DM, Weinstock DM, Pfeifer GP, Lieberman J. A PP4-phosphatase complex dephosphorylates gamma-H2AX generated during DNA replication. Mol Cell. 2008; 31:33–46. [PubMed: 18614045]

Cimprich KA, Cortez D. ATR: an essential regulator of genome integrity. Nat Rev Mol Cell Biol. 2008; 9:616–627. [PubMed: 18594563]

Clerici M, Mantiero D, Lucchini G, Longhese MP. The Saccharomyces cerevisiae Sae2 protein negatively regulates DNA damage checkpoint signalling. EMBO Rep. 2006; 7:212–218. [PubMed: 16374511]

Cobb JA, Schleker T, Rojas V, Bjergbaek L, Tercero JA, Gasser SM. Replisome instability, fork collapse, and gross chromosomal rearrangements arise synergistically from Mec1 kinase and RecQ helicase mutations. Genes Dev. 2005; 19:3055–3069. [PubMed: 16357221]

Collins SR, Schuldiner M, Krogan NJ, Weissman JS. A strategy for extracting and analyzing large-scale quantitative epistatic interaction data. Genome Biol. 2006; 7:R63. [PubMed: 16859555]

Collins SR, Miller KM, Maas NL, Roguev A, Fillingham J, Chu CS, Schuldiner M, Gebbia M, Recht J, Shales M, et al. Functional dissection of protein complexes involved in yeast chromosome biology using a genetic interaction map. Nature. 2007; 446:806–810. [PubMed: 17314980]

Downs JA, Lowndes NF, Jackson SP. A role for Saccharomyces cerevisiae histone H2A in DNA repair. Nature. 2000; 408:1001–1004. [PubMed: 11140636]

Falk JE, Chan AC, Hoffmann E, Hochwagen A. A Mec1- and PP4-dependent checkpoint couples centromere pairing to meiotic recombination. Dev Cell. 2010; 19:599–611. [PubMed: 20951350]

Fong CM, Arumugam A, Koepp DM. The Saccharomyces cerevisiae F-box protein Dia2 is a mediator of S-phase checkpoint recovery from DNA damage. Genetics. 2013; 193:483–499. [PubMed: 23172854]

Freeman AK, Monteiro AN. Phosphatases in the cellular response to DNA damage. Cell Commun Signal. 2010; 8:27. [PubMed: 20860841]

Friedel AM, Pike BL, Gasser SM. ATR/Mec1: coordinating fork stability and repair. Curr Opin Cell Biol. 2009; 21:237–244. [PubMed: 19230642]

Gingras AC, Caballero M, Zarske M, Sanchez A, Hazbun TR, Fields S, Sonenberg N, Hafen E, Raught B, Aebersold R. A novel, evolutionarily conserved protein phosphatase complex involved incisplatin sensitivity. Mol Cell Proteomics. 2005; 4:1725–1740. [PubMed: 16085932]

Guénolé A, Srivas R, Vreeken K, Wang ZZ, Wang S, Krogan NJ, Ideker T, van Attikum H. Dissection of DNA damage responses using multiconditional genetic interaction maps. Mol Cell. 2013; 49:346–358. [PubMed: 23273983]

Guillemain G, Ma E, Mauger S, Miron S, Thai R, Guérois R, Ochsenbein F, Marsolier-Kergoat MC. Mechanisms of checkpoint kinase Rad53 inactivation after a double-strand break in Saccharomyces cerevisiae. Mol Cell Biol. 2007; 27:3378–3389. [PubMed: 17325030]

Hegnauer AM, Hustedt N, Shimada K, Pike BL, Vogel M, Amsler P, Rubin SM, van Leeuwen F, Guénolé A, van Attikum H, et al. An N-terminal acidic region of Sgs1 interacts with Rpa70 and recruits Rad53 kinase to stalled forks. EMBO J. 2012; 31:3768–3783. [PubMed: 22820947]

Heideker J, Lis ET, Romesberg FE. Phosphatases, DNA damage checkpoints and checkpoint deactivation. Cell Cycle. 2007; 6:3058–3064. [PubMed: 18075314]

Hustedt N, Shimada K. Analyzing DNA replication checkpoint in budding yeast. Methods Mol Biol. 2014; 1170:321–341. [PubMed: 24906321]

Hustedt N, Gasser SM, Shimada K. Replication checkpoint: tuning and coordination of replication forks in s phase. Genes (Basel). 2013; 4:388–434. [PubMed: 24705211]

Keogh MC, Kim JA, Downey M, Fillingham J, Chowdhury D, Harrison JC, Onishi M, Datta N, Galicia S, Emili A, et al. A phosphatase complex that dephosphorylates gammaH2AX regulates DNA damage checkpoint recovery. Nature. 2006; 439:497–501. [PubMed: 16299494]

Kim ST, Lim DS, Canman CE, Kastan MB. Substrate specificities and identification of putative substrates of ATM kinase family members. J Biol Chem. 1999; 274:37538–37543. [PubMed: 10608806]

Kim JA, Hicks WM, Li J, Tay SY, Haber JE. Protein phosphatases pph3, ptc2, and ptc3 play redundant roles in DNA double-strand break repair by homologous recombination. Mol Cell Biol. 2011; 31:507–516. [PubMed: 21135129]

Lee DH, Pan Y, Kanner S, Sung P, Borowiec JA, Chowdhury D. A PP4 phosphatase complex dephosphorylates RPA2 to facilitate DNA repair via homologous recombination. Nat Struct Mol Biol. 2010; 17:365–372. [PubMed: 20154705]

Lee DH, Goodarzi AA, Adelmant GO, Pan Y, Jeggo PA, Marto JA, Chowdhury D. Phosphoproteomic analysis reveals that PP4 dephosphorylates KAP-1 impacting the DNA damage response. EMBO J. 2012; 31:2403–2415. [PubMed: 22491012]

Lee DH, Acharya SS, Kwon M, Drane P, Guan Y, Adelmant G, Kalev P, Shah J, Pellman D, Marto JA, Chowdhury D. Dephosphorylation enables the recruitment of 53BP1 to double-strand DNA breaks. Mol Cell. 2014; 54:512–525. [PubMed: 24703952]

Leroy C, Lee SE, Vaze MB, Ochsenbein F, Guerois R, Haber JE, Marsolier-Kergoat MC. PP2C phosphatases Ptc2 and Ptc3 are required for DNA checkpoint inactivation after a double-strand break. Mol Cell. 2003; 11:827–835. [PubMed: 12667463]

Lisby M, Barlow JH, Burgess RC, Rothstein R. Choreography of the DNA damage response: spatiotemporal relationships among checkpoint and repair proteins. Cell. 2004; 118:699–713. [PubMed: 15369670]

Liu S, Shiotani B, Lahiri M, Maréchal A, Tse A, Leung CC, Glover JN, Yang XH, Zou L. ATR autophosphorylation as a molecular switch for checkpoint activation. Mol Cell. 2011; 43:192–202. [PubMed: 21777809]

Ma H, Han BK, Guaderrama M, Aslanian A, Yates JR 3rd, Hunter T, Wittenberg C. Psy2 targets the PP4 family phosphatase Pph3 to dephosphorylate Mth1 and repress glucose transporter gene expression. Mol Cell Biol. 2014; 34:452–463. [PubMed: 24277933]

Mailand N, Bekker-Jensen S, Bartek J, Lukas J. Destruction of Claspin by SCFbetaTrCP restrains Chk1 activation and facilitates recovery from genotoxic stress. Mol Cell. 2006; 23:307–318. [PubMed: 16885021]

Mordes DA, Glick GG, Zhao R, Cortez D. TopBP1 activates ATR through ATRIP and a PIKK regulatory domain. Genes Dev. 2008; 22:1478–1489. [PubMed: 18519640]

Nakada S, Chen GI, Gingras AC, Durocher D. PP4 is a gamma H2AX phosphatase required for recovery from the DNA damage checkpoint. EMBO Rep. 2008; 9:1019–1026. [PubMed: 18758438]

Nam EA, Zhao R, Glick GG, Bansbach CE, Friedman DB, Cortez D. Thr-1989 phosphorylation is a marker of active ataxia telangiectasiamutated and Rad3-related (ATR) kinase. J Biol Chem. 2011; 286:28707–28714. [PubMed: 21705319]

O'Neill BM, Szyjka SJ, Lis ET, Bailey AO, Yates JR 3rd, Aparicio OM, Romesberg FE. Pph3-Psy2 is a phosphatase complex required for Rad53 dephosphorylation and replication fork restart during recovery from DNA damage. Proc Natl Acad Sci USA. 2007; 104:9290–9295. [PubMed: 17517611]

Ohouo PY, Bastos de Oliveira FM, Liu Y, Ma CJ, Smolka MB. DNA-repair scaffolds dampen checkpoint signalling by counteracting the adaptor Rad9. Nature. 2013; 493:120–124. [PubMed: 23160493]

Osborn AJ, Elledge SJ. Mrc1 is a replication fork component whose phosphorylation in response to DNA replication stress activates Rad53. Genes Dev. 2003; 17:1755–1767. [PubMed: 12865299]

Paciotti V, Clerici M, Lucchini G, Longhese MP. The checkpoint protein Ddc2, functionally related to S. pombe Rad26, interacts with Mec1 and is regulated by Mec1-dependent phosphorylation in budding yeast. Genes Dev. 2000; 14:2046–2059. [PubMed: 10950868]

Paciotti V, Clerici M, Scotti M, Lucchini G, Longhese MP. Characterization of mec1 kinase-deficient mutants and of new hypomorphic mec1 alleles impairing subsets of the DNA damage response pathway. Mol Cell Biol. 2001; 21:3913–3925. [PubMed: 11359899]

Papamichos-Chronakis M, Peterson CL. The Ino80 chromatinremodeling enzyme regulates replisome function and stability. Nat Struct Mol Biol. 2008; 15:338–345. [PubMed: 18376411]

Pasero P, Braguglia D, Gasser SM. ORC-dependent and origin-specific initiation of DNA replication at defined foci in isolated yeast nuclei. Genes Dev. 1997; 11:1504–1518. [PubMed: 9203578]

Peschiaroli A, Dorrello NV, Guardavaccaro D, Venere M, Halazonetis T, Sherman NE, Pagano M. SCFbetaTrCP-mediated degradation of Claspin regulates recovery from the DNA replication checkpoint response. Mol Cell. 2006; 23:319–329. [PubMed: 16885022]

Piston DW, Kremers GJ. Fluorescent protein FRET: the good, the bad and the ugly. Trends Biochem Sci. 2007; 32:407–414. [PubMed: 17764955]

Shimada K, Pasero P, Gasser SM. ORC and the intra-S-phase checkpoint: a threshold regulates Rad53p activation in S phase. Genes Dev. 2002; 16:3236–3252. [PubMed: 12502744]

Shimada K, Oma Y, Schleker T, Kugou K, Ohta K, Harata M, Gasser SM. Ino80 chromatin remodeling complex promotes recovery of stalled replication forks. Curr Biol. 2008; 18:566–575. [PubMed: 18406137]

Smolka MB, Albuquerque CP, Chen SH, Zhou H. Proteomewide identification of in vivo targets of DNA damage checkpoint kinases. Proc Natl Acad Sci USA. 2007; 104:10364–10369. [PubMed: 17563356]

Sobhian B, Shao G, Lilli DR, Culhane AC, Moreau LA, Xia B, Livingston DM, Greenberg RA. RAP80 targets BRCA1 to specific ubiquitin structures at DNA damage sites. Science. 2007; 316:1198–1202. [PubMed: 17525341]

Szyjka SJ, Aparicio JG, Viggiani CJ, Knott S, Xu W, Tavaré S, Aparicio OM. Rad53 regulates replication fork restart after DNA damage in Saccharomyces cerevisiae. Genes Dev. 2008; 22:1906–1920. [PubMed: 18628397]

Tercero JA, Longhese MP, Diffley JF. A central role for DNA replication forks in checkpoint activation and response. Mol Cell. 2003; 11:1323–1336. [PubMed: 12769855]

Travesa A, Duch A, Quintana DG. Distinct phosphatases mediate the deactivation of the DNA damage checkpoint kinase Rad53. J Biol Chem. 2008; 283:17123–17130. [PubMed: 18441009]

van Attikum H, Fritsch O, Hohn B, Gasser SM. Recruitment of the INO80 complex by H2A phosphorylation links ATP-dependent chromatin remodeling with DNA double-strand break repair. Cell. 2004; 119:777–788. [PubMed: 15607975]

Van Hoof C, Martens E, Longin S, Jordens J, Stevens I, Janssens V, Goris J. Specific interactions of PP2A and PP2A-like phosphatases with the yeast PTPA homologues, Ypa1 and Ypa2. Biochem J. 2005; 386:93–102. [PubMed: 15447631]

Vizcaino JA, Deutsch EW, Wang R, Csordas A, Reisinger F, Rios D, Dianes JA, Sun Z, Farrah T, Bandeira N, et al. ProteomeXchange provides globally coordinated proteomics data submission and dissemination. Nat Biotechnol. 2014; 32:223–226. [PubMed: 24727771]

Wang H, Gao J, Wong AH, Hu K, Li W, Wang Y, Sang J. Rfa2 is specifically dephosphorylated by Pph3 in Candida albicans. Biochem J. 2013; 449:673–681. [PubMed: 23140133]

Yamagoe S, Kanno T, Kanno Y, Sasaki S, Siegel RM, Lenardo MJ, Humphrey G, Wang Y, Nakatani Y, Howard BH, Ozato K. Interaction of histone acetylases and deacetylases in vivo. Mol Cell Biol. 2003; 23:1025–1033. [PubMed: 12529406]

Zhang W, Durocher D. De novo telomere formation is suppressed by the Mec1-dependent inhibition of Cdc13 accumulation at DNA breaks. Genes Dev. 2010; 24:502–515. [PubMed: 20194442]

Zhao X, Muller EG, Rothstein R. A suppressor of two essential checkpoint genes identifies a novel protein that negatively affects dNTP pools. Mol Cell. 1998; 2:329–340. [PubMed: 9774971]

Zou L, Elledge SJ. Sensing DNA damage through ATRIP recognition of RPA-ssDNA complexes. Science. 2003; 300:1542–1548. [PubMed: 12791985]

Highlights

- S phase functions of Mec1 kinase are balanced by phosphatase Pph3-Psy2
- Mec1-Ddc2 binds PP4 (Pph3-Psy2) through a Ddc2-Psy2 interaction site
- The two complexes colocalize at foci of stalled replication forks
- Most *mec1-100*-sensitive phosphorylation events on HU are PP4 targets

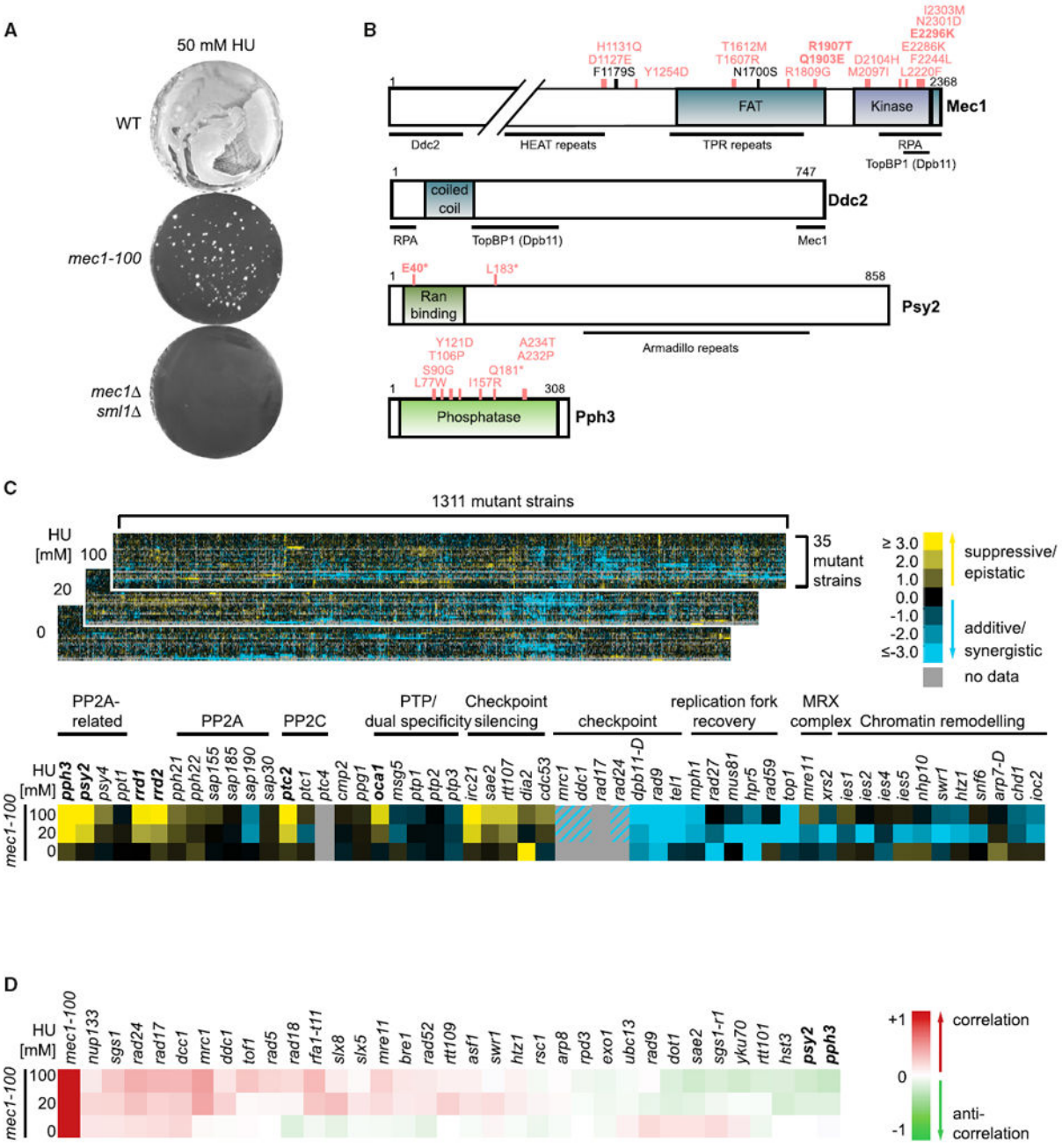

Figure 1. Mutations in *PSY2* and *PPH3* Genes Suppress *mec1-100* HU Sensitivity

(A) The indicated strains (see Tables S1 and S2) were plated on YPAD + 50 mM HU for 3 days at 30°C. Colonies appear white on dark background.

(B) Mec1, Ddc2, Psy2, and Pph3 domain architecture with *mec1-100* mutations in black and *mec1-100* suppressor mutations in red. Bold, mutations found more than once independently. Asterisks, STOP codon at indicated residue or frameshift (aa 181) resulting in STOP at aa 183 (GA-6610).

(C) Upper panel, overview of genetic interaction screen (E-MAP; full data in Table S4), 35 mutant "query" strains combined with 1,525 mutant strains (1,311 after quality control), see

Table S3. Double mutant growth was scored on 0, 20, and 100 mM HU. Genetic interaction scoring is at right. Hatching indicates “no data” in E-MAP, but confirmed negative interaction by drop assay (see Figure S1E). Lower panel, selected *mec1-100* genetic interactions, including phosphatase mutants (significant positive interaction with *mec1-100* are in bold). DAmP allele = D. Complete *mec1-100* genetic interactions are in Figure S1. (D) Heat map of Pearson correlation coefficients for *mec1-100* genetic interaction profile with those of the other strains on 0, 20, and 100 mM HU. Correlation coding is at right.

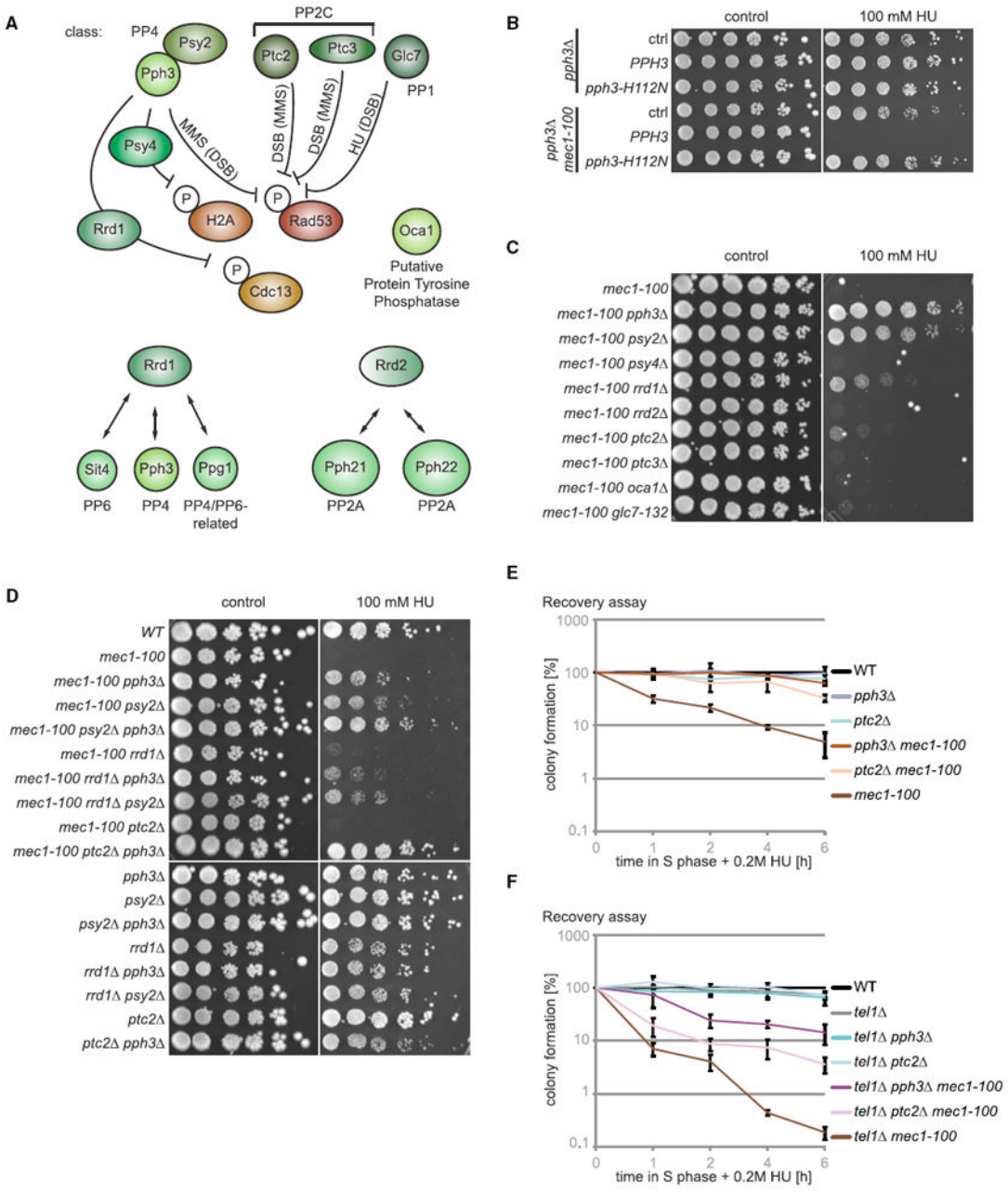

Figure 2. Validation of *psy2Δ* and *pph3Δ* as Suppressors of *mec1-100* HU Sensitivity

(A) Scheme of yeast phosphatases and relationships with *mec1-100* or checkpoint downregulation roles, see text.

(B) *pph3*Δ or *pph3*Δ *mec1-100* cells with *TRP1*-based control plasmid or plasmids expressing *PPH3* or *pph3-H112N* from *PPH3* promoter. Cells grown in synthetic complete medium (lacking tryptophan) (SC-TRP) in a 5-fold dilution series on SC-TRP ±100 mM HU.

(C) A 5-fold dilution series on YPAD ±100 mM HU of isogenic strains with indicated genotypes (see Tables S1 and S2).

(D) Isogenic strains with indicated genotypes were treated as in (C).

(E) Recovery from replication fork stalling was monitored as colony outgrowth of cells after synchronization in G1 by α factor and release into S phase with 0.2 M HU for indicated times. Genotypes of isogenic strains are indicated in Tables S1 and S2. Error bars indicate SD.

(F) Isogenic strains with indicated genotypes were treated as in (E).

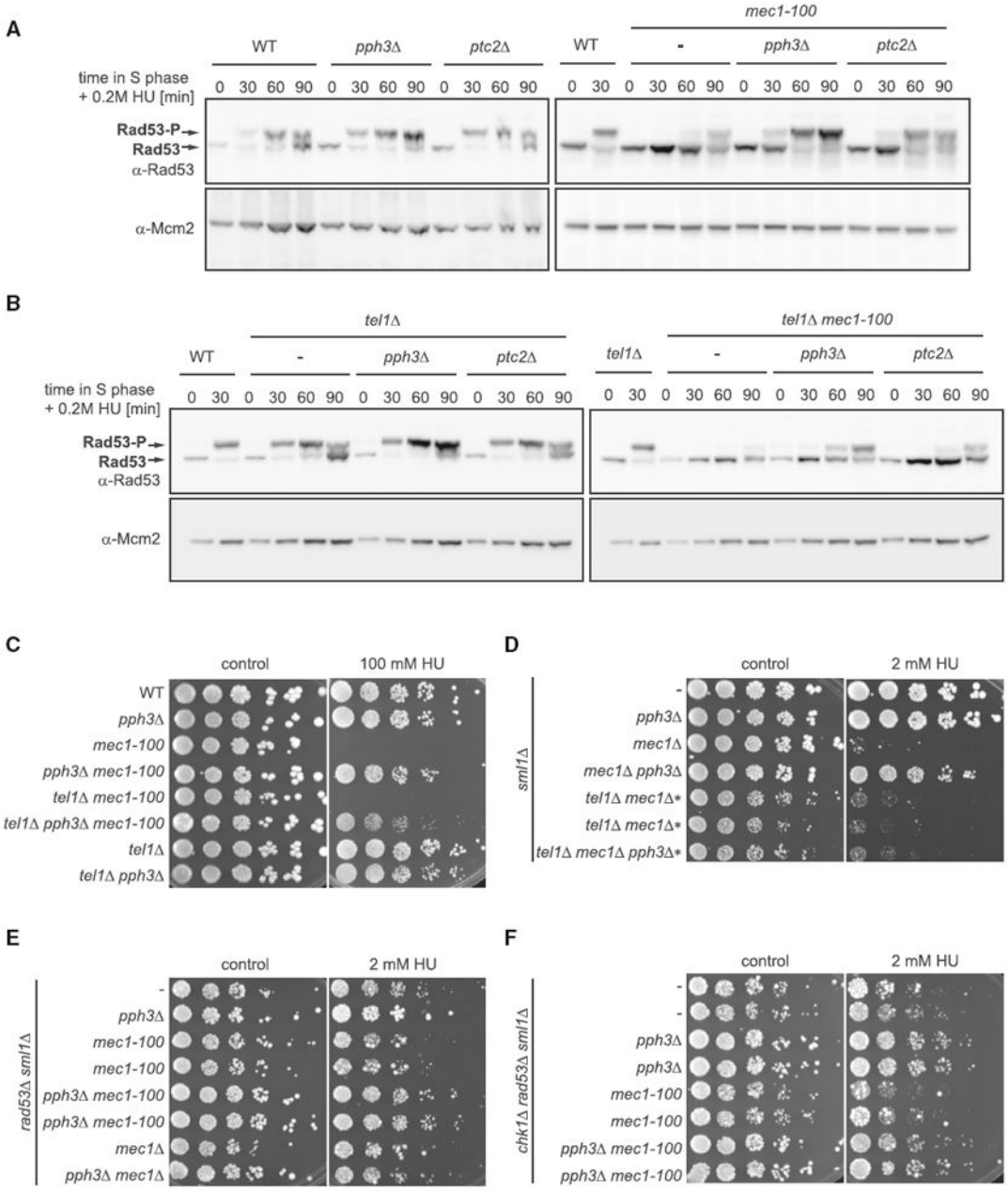

Figure 3. Suppression of *mec1-100* Correlates with Rad53 Activation

(A) Rad53 phosphorylation monitored by western blot after synchronization in G1 (α factor) and release for the indicated times into 0.2 M HU. Genotypes of isogenic strains are indicated in Tables S1 and S2.

(B) Isogenic strains as indicated (see Tables S1 and S2) were treated as in (A).

(C) A 5-fold dilution series on YPAD ±100 mM HU. Genotypes of isogenic strains are indicated in Tables S1 and S2.

(D) A 5-fold dilution series of isogenic strains as indicated on YPAD ±2 mM HU. Asterisk, 10× more cells plated.

(E) Isogenic strains with indicated genotypes were treated as in (D).

(F) Isogenic strains with indicated genotypes were treated as in (D). See Figure S2; Tables S1 and S2.

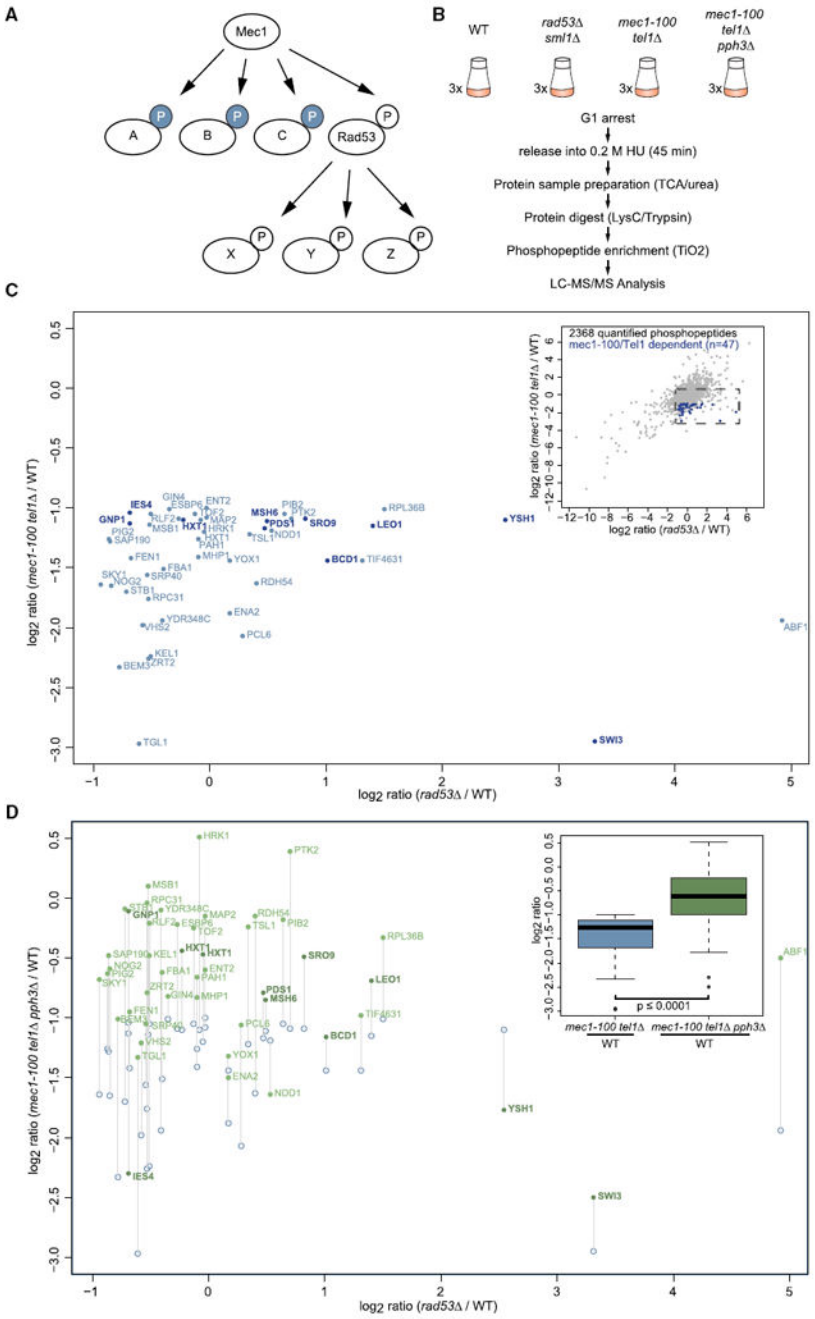

Figure 4. Most mec1-100-Regulated Phosphopeptides Are Upregulated by Pph3 Loss

(A) Scheme of Mec1-dependent and Rad53-independent phosphorylation sites.

(B) Phosphoproteomics experimental scheme, in which three cultures of each indicated strain (see Tables S1 and S2) were synchronized in G1 and released 45 min in 0.2 M HU. Phosphoproteomics sample preparation is in Supplemental Experimental Procedures.

(C) Phosphopeptide abundances ($\log_2$ ratio [mutant/WT]) in *mec1-100 tel1*Δ cells plotted against abundances in *rad53*Δ *sml1*Δ. Shown are mec1-100/Tel1 specific phosphopetides which have a $\log_2$ ratio ≤−1 for *mec1-100 tel1*Δ / WT ($p \leq 0.05$, Student's paired t test over three replicates) and $\log_2$ ratio ≥−1 for *rad53*Δ *sml1*Δ / WT. Full list in Table S6.

Phosphopeptides modified on p[S/T]Q consenses are in dark blue and bold, labeled by protein names. Inlay, plotting of indicated ratios of all quantified phosphopeptides (Table S5). Blue, mec1-100/Tel1 specific phosphopeptides.

(D) Plotting of phosphopeptide abundances (log_2 ratio [mutant/WT]) in *mec1-100 tel1*Δ *pph3*Δ cells against phosphopeptide abundances in *rad53*Δ *sml1*Δ cells of phosphopeptides used in (C). Blue circles indicate position in previous plot (C), and gray lines connect same phosphopeptides. Inlay, Tukey boxplot of ratios of mec1-100/tel1-specific phosphopeptides and p values calculated by one-tailed Wilcoxon signed rank test. See Figure S3.

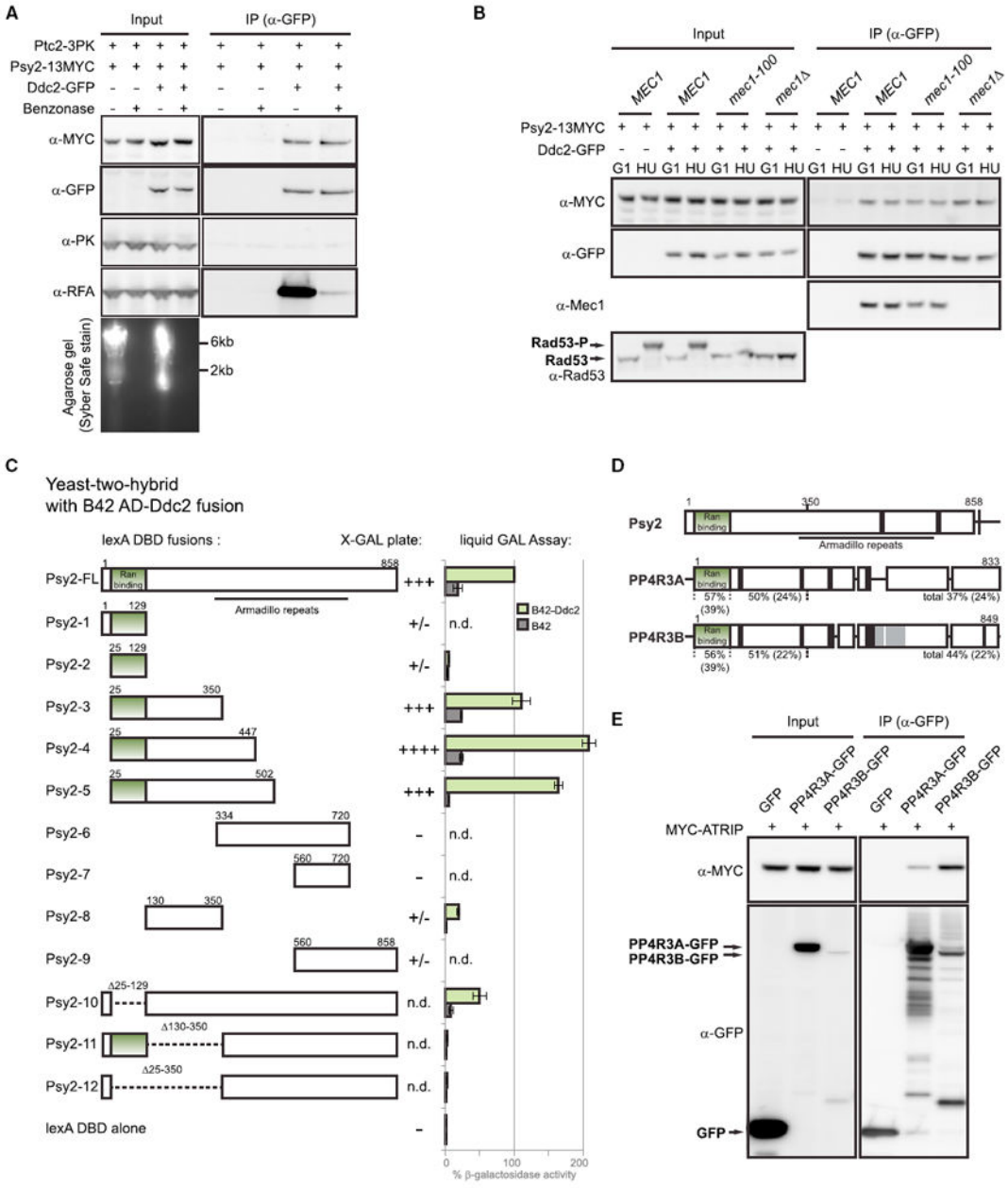

Figure 5. Ddc2 and Psy2 Interact Physically

(A) Native extracts from cycling cultures of indicated strains (see Tables S1 and S2) ± RNaseA and benzonase treatment were subjected to anti-GFP IP and western blotting with indicated antibodies. Nucleic acid digestion in GFP-depleted extracts after IP was analyzed by agarose gel and SYBR Safe.

(B) Cells of indicated genotypes (see Tables S1 and S2) were arrested in G1 by α factor and held or released into 0.2M HU for 30 min. Extracts were subjected to anti-GFP IP and western blotting with indicated antibodies.

(C) Y2H analysis of *DDC2* fused to B42-AD and *PSY2* fragments fused to lexA-DBD. Bars indicate β-galactosidase activity (error bars represent SD); symbols indicate color on X-GAL plate (raw data in Figure S5C). Dubious interaction (±) and not determined (n.d.).
(D) Scheme of Clustal Omega multiple sequence alignment of Psy2 (P40164), PP4R3A (Q6IN85-1), and PP4R3B (Q5MIZ7-1). Vertical lines, alignment gaps ≥5 aa; gray, region missing in clone Q5MIZ7-3, used in (E). The % sequence similarity (in brackets % identity) calculation based on *PSY2* length or length of indicated fragments.
(E) HEK293T cells were transfected with plasmids expressing MYC-ATRIP (#3,525) and GFP (#3,493), PP4R3A-GFP (#3,518), or PP4R3B-GFP (#3,588). Native extracts at 48 hr post transfection were subjected to anti-GFP IP and western blotting as indicated. See Figures S4 and S5.

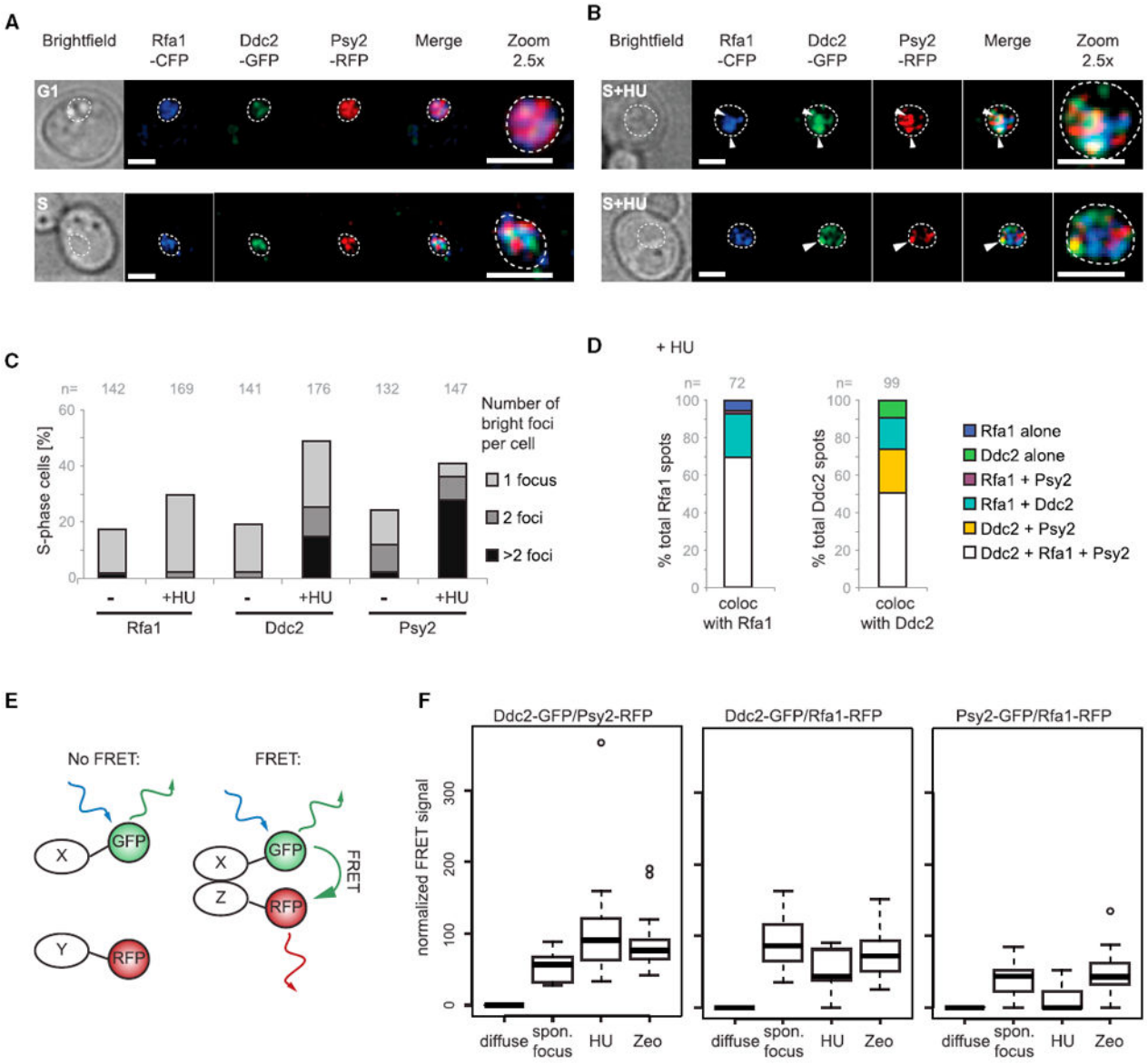

Figure 6. Ddc2-GFP and Psy2-RFP Foci Colocalize and Show FRET Signals

(A–D) *RFA1-CFP DDC2-GFP PSY2-RFP* cells were incubated ±0.2 M HU for 1 hr prior to fixation for microscopy. (A) Images of untreated G1 and S phase cells showing indicated fluorescence channels. Bar, 2 μm. Dashed line encircles cell nucleus. (B) Examples of HU-treated cells showing colocalization of all three proteins in two foci (upper panel), or of colocalization of Ddc2 and Psy2 only (lower panel). Arrowheads = foci.

(C) Quantification of bright focus number per S phase cell. (D) Colocalization of Rfa1 and Ddc2 spots with indicated protein after HU treatment.

(E) Schematic of FRET principle, GFP and RFP must be within 10 nm for RFP emission.

(F) *DDC2-GFP PSY2-RFP, DDC2-GFP RFA1-RFP*, and *PSY2-GFP RFA1-RFP* cells treated 1 hr ± 0.2 M H U or 400 μg/ml Zeocin prior to fixation, were analyzed for FRET-induced RFP signals at bright GFP foci (“focus”) or in the nucleus without a focus

("diffuse"). Because Rfa1-RFP cells showed slight sensitivity to MMS (Figure S4F), low FRET signals were confirmed with Rfa2-GFP/Psy2-RFP (data not shown). See Figure S6.

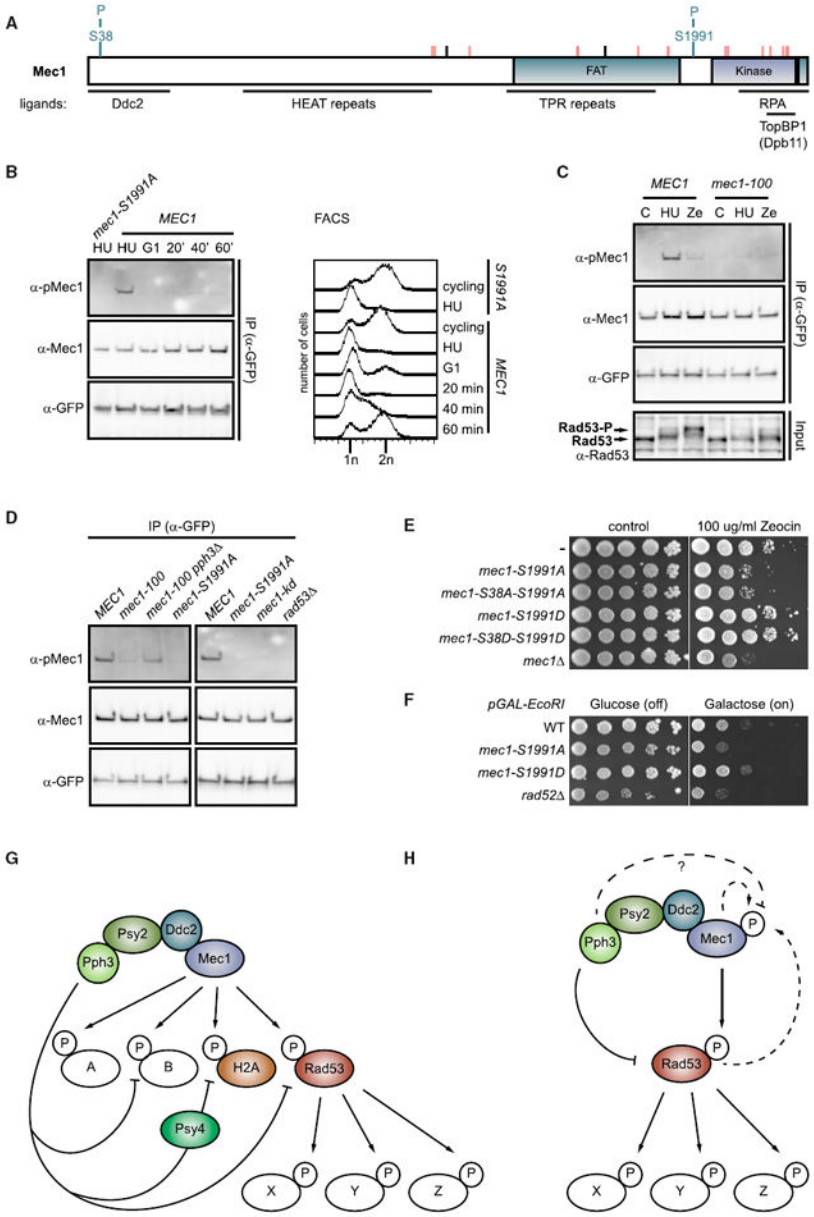

Figure 7. Mec1 Phosphoserine 1991 Is Regulated by Rad53 and Pph3

(A) Mec1 phosphosites in blue, black lines = *mec1-100* mutations, and red lines = suppressor mutations (Figure 1), and interaction domains and structural domains indicated below.

(B) *Ddc2-GFP* and *Ddc2-GFP mec1-S1991A* cells were treated with 0.2MHU for 1 hr or arrested in G1 and released into YPAD at 25°C for indicated times. FACS was performed on samples to confirm cell cycle stages. After IP with α-GFP, western blots were performed with indicated antibodies, e.g., α-pMec1 (Mec1 phosphoserine 1991).

(C) Exponential cultures of *Ddc2-GFP* and *Ddc2-GFP mec1-100* ±0.2 M HU or 400 μg/ml Zeocin for 1 hr were extracted and subjected to IP by α-GFP. Western blots were probed

with indicated antibodies, and input samples were probed with α-Rad53 to monitor checkpoint activation.

(D) Native extracts were prepared from *Ddc2-GFP* strains with indicated genotypes (see Tables S1 and S2) after 1 hr incubation + 0.2MHU. α-GFP IP and western blotting with indicated antibodies was performed.

(E) 10-fold dilution series on YPAD ±100 μg/ml Zeocin of isogenic strains of indicated genotypes (see Tables S1 and S2).

(F) Cells transformed with pGAL-EcoRI (#2,745) and grown in selective medium to ensure plasmid retention were plated on 2% glucose or galactose supplemented with 2% raffinose, in 10-fold dilution series.

(G) Model of Ddc2-Psy2 interaction and coordinated interplay of Mec1-Ddc2 and Pph3-Psy2. Both target Rad53, H2A, and other targets. Most mec1-100/Tel1-specific phosphosites are regulated by Pph3-Psy2 (“B”), while a few are not (“A”).

(H) Mec1 phosphoserine 1991 requires Rad53 and Mec1, is compromised in *mec1-100* cells, and rescued by loss of Pph3-Psy2. Mec1 regulation of Mec1 may be indirect. See Figure S7.